 MCB, vol.4, no.1, pp.41-53, 2007

Numerical Simulations of Pulsatile Flow in an End-to-Side Anastomosis Model

E. Shaik*, K.A. Hoffmann* and J-F. Dietiker*

Abstract: A potential interaction between the local hemodynamics and the artery wall response has been suggested for vascular graft failure by intimal hyperplasia (IH). Among the various hemodynamic factors, wall shear stress has been implicated as the primary factor responsible for the development of IH. In order to explore the role of hemodynamics in the formation of IH in end-to-side anastomosis, computational fluid dynamics is employed. To validate the numerical simulations, comparisons with existing experimental data are performed for both steady and pulsatile flows. Generally, good agreement is observed with the velocity profiles whereas some discrepancies are found in wall shear stress (WSS) distributions. Using the same end-to-side anastomosis geometry, numerical simulations are extended using a femoral artery waveform to identify the possible role of unsteady hemodynamics. In the current simulations, Carreau-Yasuda model is used to account for the non-Newtonian nature of blood. Computations indicated a disturbed flow field at the artery-graft junction leading to locally elevated shear stresses on the vascular wall. Furthermore, the shear stress distribution followed the same behavior with oscillating magnitude over the entire flow cycle. Thus, distal IH observed in end-to-side artery-graft models may be caused by the fluctuations in WSS's along the wall.

Keyword: Artery bypass, computational fluid dynamics, end-to-side anastomosis, hemodynamics, intimal hyperplasia.

1 Introduction

When the natural vessel fails, vascular grafts are commonly used to bypass a diseased vessel, enabling an adequate supply of blood to be restored to distal tissues and organs. If possible, the best choice for a replacement vessel is an autograft (autogenous saphenous vein), where sections of the patient's healthy blood vessels (usually veins) are harvested and implanted at the required locations. However, patients with pre-existing vascular disease or patients that have already had autograft procedures, may not have blood vessels that are sufficiently healthy to adequately serve as replacements. In such cases, the most common form of treatment has been the use of synthetic polymeric materials such as, ePTFE (extended polytetrafluoroethylene) or Dacron (polyethylene terephthalate) [Ku and Allen (1995)], to form permanent replacements for the damaged vessels.

Anastomotic IH, especially at the distal end-to-side anastomosis, is one of the major causes of failure of arterial bypass grafts [Dilley, McGeachie and Prendergast (1988)], [Echave, Koornick and Haimov (1979)]. This disease is characterized by a progressive thickening of the inner most layer of the artery wall in the region where the graft is joined to the artery. As a result, gradual narrowing of the vessel leads to a blockage of the vessel. IH is more prevalent at the distal anastomosis of an end-to-side graft, where the flow is more disturbed rather than at the proximal anastomosis [Sottiurai, Yao, Baston, Sue, Jones Nakamura (1989)].

Although there are several theories in the literature, the exact cause of IH is uncertain [Dilley, McGeachie and Prendergast (1988)], [Clowes, Kirkman and Clowes (1986)], [Bandyk, Seabrook, and Moldenhauer (1988)], [Clowes, and Clowes (1980)]. The development of IH in bypass grafts depends on several factors such as injury, hemodynamics, and graft-artery com-

* Wichita State University, Wichita, KS, USA.

pliance mismatch. The fluid dynamics within the vascular grafts (hemodynamics) is widely believed to play an important role in the initiation and development of anastomotic IH [Dobrin, Littooy and Endean (1989)], [Rittgers and Karayannacos (1978)], [Chevru, and Moore (1990)]. However, the specific mechanism(s) whereby blood flow patterns influence the development of IH remains a major unsolved question in bioengineering. In the past, a variety of hemodynamic factors have been proposed in the development of IH, which includes recirculating zones, turbulence, low and oscillating shear stress (OSS), temporal and spatial variations of the wall shear stress (WSS). However, to determine the exact influence of these factors, quantitative hemodynamic information is required. Several experimental and computational studies have been performed to investigate the correlation between distal anastomotic IH and hemodynamics. Various experimental techniques such as ultrasound Doppler techniques in vitro and in vivo [Rittgers and Bhambhani (1991)], [Keynton, Evancho, Sims and Rittgers (1999)], Laser-Doppler anemometry measurements of flow visualizations in vitro [Keynton, Rittgers and Shu (1991)], [Loth, Jones, Giddens, Bassiouny, Zarins and Glagov (1997)] and photochromic dye tracer in vivo [Steinman, Vinh, Ethier, Ojha, Cobbold and Johnston (1993)] have been employed by researchers for quantitative flow measurements. With the expansion of Computational Fluid Dynamics (CFD), investigators have used various numerical methods, such as Finite Element Method (FEM), Finite Difference Method (FDM) and Finite Volume Method (FVM) to solve the respective flow equations and to perform a detailed flow field analysis with respect to the arterial blood flow.

Pietrabissa, Inzoli and Fumero (1990), simulated steady Newtonian blood flow in an aorta-coronary bypass model while Perktold, Tatzl and Schima (1993), simulated pulsatile non-Newtonian blood flow. In both of these investigations, a separated flow region at the toe of the anastomosis was observed. Ojha (1993), Ojha, Ethier, Johnston and Cobbold (1990) found regions of low WSS at the heel and toe of the anastomosis along with sharp temporal and spatial variations of WSS along the floor of the artery. Similarly, Bassiouny, White, Glagov, Choi, Giddens and Zarins (1992), observed a stagnation zone along the floor of the artery, while separated and secondary flows occurred at the heel and toe of the graft. Bharadvaj and Daddario (1982), indicated that IH is greater in regions of flow separation and that the distal anastomosis was more susceptible to hyperplastic lesions than the proximal junction. Fei, Thomas and Rittgers (1994), investigated the effect of artery-graft angle and flow rate upon hemodynamics in distal vascular graft anastomoses. Henry, Collins, Hughes and How (1996), showed that the regions corresponding to IH formation in an end-to-side anastomosis had low WSS with increased spatial wall shear stress gradients (WSSG). Lei, Archie, and Kleinstreuer (1997), (1996) performed pulsatile flow simulations in various end-to-side anastomosis models and calculated WSS, WSSG and OSS and correlated the formation of the IH with respect to these parameters. More recently, Yang, Tang, and Liu (2003), simulated an end-to-end anastomosis model with tube wall growth and fluid-structure interactions in rat abdominal artery with a vein graft. In that investigation they related the low and oscillating WSS for the development of focal IH and restenosis.

Among the end-to-side anastomosis studies reviewed, hemodynamic predictor of IH formation has not been agreed upon by various researchers. This is primarily due to the lack of uniform treatment of the flow conditions. Furthermore, among these studies the comparison of numerical results with experimental data has either not been conducted or has been conducted in a simplified vitro models using various flow visualization methods. To verify the validity and versatility of numerical simulations, quantitative comparisons between numerical results and experimental data in real geometries are needed. A quantitative comparison of WSS under the same model geometry would help to better delineate the hemodynamic characteristics and identify the important mechanical factor(s) that may be involved in the formation of IH. Therefore, the current study was per-

formed with the goal of identifying those hemodynamic characteristics that could potentially lead to IH.

In this study, the finite volume method has been employed in the numerical simulation of an end-to-side anastomosis model. First, results for the steady and pulsatile Newtonian fluid flow in a two-dimensional (2-D) rigid walled end-to-side anastomosis model are compared with the experimental measurements of Steinman, Vinh, Ethier, Ojha, Cobbold and Johnston (1993) in terms of velocity profiles and WSS variations. Subsequently, the simulations are extended to three-dimensions to gain a qualitative understanding of the flow and WSS behavior. The same end-to-side geometry with a mid-femoral waveform as measured by Doppler ultrasonography [Steinman, Vinh, Ethier, Ojha, Cobbold and Johnston (1993)] is used along with the Carreau-Yasuda model to account for the non-Newtonian property of blood.

2 Model geometry

Steinman, Vinh, Ethier, Ojha, Cobbold and Johnston (1993), developed an in vitro model of an end-to-side anastomosis and performed photochromic dye tracer measurements of velocity fields under steady and pulsatile flow conditions. The model consisted of a two-dimensional flow channel constructed from ultraviolet-transparent plexiglas. The end-to-side anastomosis model had a channel height of 5 mm, a width of 50 mm, an entrance length of 190 mm, and a graft-vessel angle of 45 degrees. Extensive velocity measurements were performed, and the wall shear stresses were estimated from the slope of the near-wall velocity profiles. Thus, this study provides a well-defined set of experimental data with which numerical results may be compared. The model used in the experimental study of Steinman, Vinh, Ethier, Ojha, Cobbold and Johnston (1993), was purposely designed to have a mathematically described geometry to allow direct translation to a numerical model. The mathematical description of the geometry was used to generate the computational model used in this study. Details of the model geometry, the experimental setup and the measurement technique are found in [Steinman, Vinh, Ethier, Ojha, Cobbold and Johnston (1993)]. The model geometry and the nomenclature used in this study are shown in Fig 1. GAMBIT [Fluent Inc. Lebanon, NH] is used to develop geometrical models of two and three-dimensional end-to-side anastomosis which are shown in Figs. 2 and 3 respectively. For the mesh generation, four-node quad elements were used to mesh the 2-D model whereas for 3-D model tetrahedral elements were used. The optimal number of elements was determined from the mesh-independence study.

The 2-D meshed model consisted of 10,780 elements and 11,124 nodes, while the 3-D model consisted of 151,378 elements and 62,792 nodes. The meshes were clustered near the arterial wall to produce a greater accuracy in calculating the shear stress.

3 Governing equations

The governing equations are the conservations of mass and momentum for an unsteady, incompressible and, isothermal flow. They are presented using tensor notation as follows.

$$u_{i,i} = 0 \tag{1}$$

$$\rho \left(\frac{\partial u_i}{\partial t} + u_j u_{i,j} \right) = -p_{,i} + \tau_{ij,j} \tag{2}$$

Where ρ is the density, u is the velocity vector, t is the time, and p is the pressure.

The shear stress tensor τ_{ij} is defined by the constitutive equation:

$$\tau_{ij} = \eta \dot{\gamma}_{ij} \tag{3}$$

There are various models available in the literature to describe the non-Newtonian behavior of blood, e.g., Casson model [Chien, Usami and Richard (1984)] and Simpler model [Quemada (1977)]. Yeleswarapu (1996), provides a detailed report on these models. In the current investigation, the complex rheological behavior of blood is approximated using the shear-thinning Carreau-Yasuda model [Shaik, Hoffmann and Dietiker (2006)], [Gijsen, Van de Vosse and Janssen

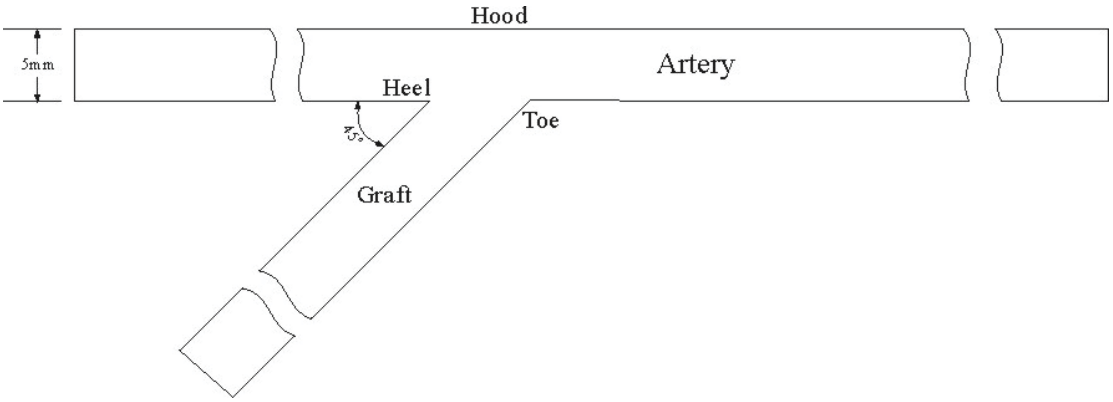

Figure 1: Geometry of end-to-side anastomosis

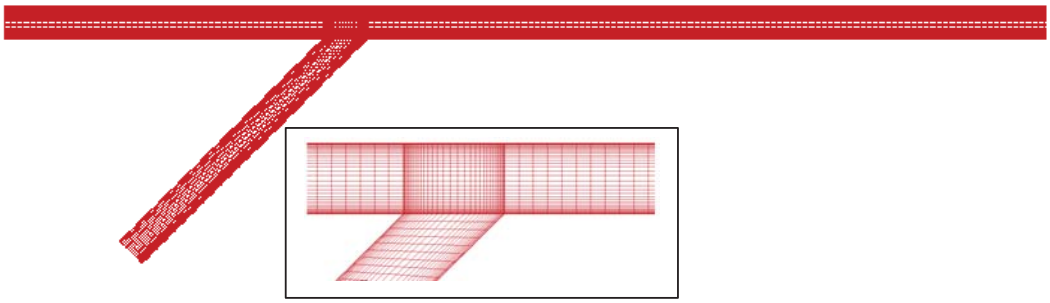

Figure 2: Grid system of the 2-D end-to-side anastomosis. The inset shows the enlarged view of the mesh at the junction of the anastomosis

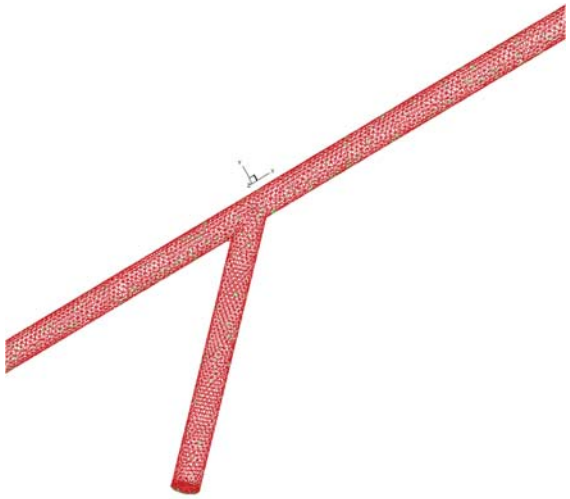

Figure 3: Perspective view of the 3-D end-to-side anastomosis

(1999)] where the apparent viscosity is expressed as a function of the shear rate as

$$\frac{\eta-\eta_\infty}{\eta_0-\eta_\infty}=[1+(\lambda\dot{\gamma})^a]^{(n-1)/a} \tag{4}$$

Where $\dot{\gamma}$ is the shear rate, η_∞ is the viscosity at infinite shear rates, η_0 is the zero shear rate viscosity, λ is the relaxation time in seconds and parameters a and n can be varied to match the shear thinning behavior of blood. Experimentally correlated model parameters for the Carreau-Yasuda model are taken from [Gijsen, Van de Vosse and Janssen (1999)] and are:

$$\eta_\infty = 2.2\times10^{-3}\text{Pa}\cdot\text{s}, \quad \eta_0 = 22\times10^{-3}\text{Pa}\cdot\text{s},$$
$$n = 0.392, \quad \lambda = 0.110\text{s},$$
$$a = 0.644$$

4 Numerical approach

FLUENT [Fluent Inc. Lebanon, NH], a commercially available CFD code, which is based on fi-

nite volume method, was used to solve the governing equations in all the simulations. The momentum equations are approximated by second-order central-differencing discretization scheme. The pressure-velocity coupling is accomplished through the SIMPLE algorithm. In the simulations, segregated solver with implicit time setting formulation was used, which solves the governing equations in a decoupled approach. To account for the non-Newtonian property of blood based on Carreau-Yasuda model, a user-defined function was developed.

In the present simulations, rigid wall conditions were assumed since synthetic grafts and diseased arteries are expected to be relatively stiff. The assumption of no flow through proximal end of the host artery is also imposed which corresponds to the implantation of graft in a severely stenosed artery. The lengths of the graft and the artery were made sufficiently long so as to reduce the velocity oscillations in the solutions, to produce fully developed flow, and to accurately manage the larger Reynolds numbers and negative flow rates encountered when using the mid-femoral waveform.

For the unsteady cases, a total of 1000 uniform time steps per cardiac cycle were used. The time marching procedure was carried out until steady oscillatory motion was achieved. To eliminate the start effect of pulsatile flows, the simulation was carried out over three full cycles. The typical CPU time per cycle was about 7 hours for 2-D and 82 hours for 3-D models, using a Pentium dual core processor of 3.2GHz with 3.0 GB Ram.

5 Boundary conditions

5.1 2-D anastomosis

For steady flow, a Reynolds number of 130 with kinematic and dynamic viscosities of 1.89 cStokes and 1.43 cPoise respectively were used at the graft inlet.

For unsteady flow, a flow waveform was specified at the graft inlet. Figure 4 illustrates the flow waveform measured at the graft inlet in the vitro experiment. The data points in Fig.4 correspond to the vitro experiments which are spline-fitted in order to use them as the inlet condition for the numerical analysis.

No-slip conditions were imposed on all the walls and a zero gauge pressure and zero axial velocity gradients are specified at the distal outlet of the artery.

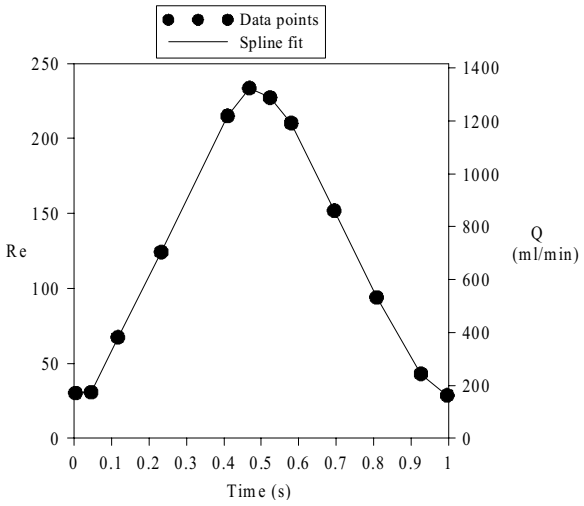

Figure 4: Flow waveform at the graft inlet

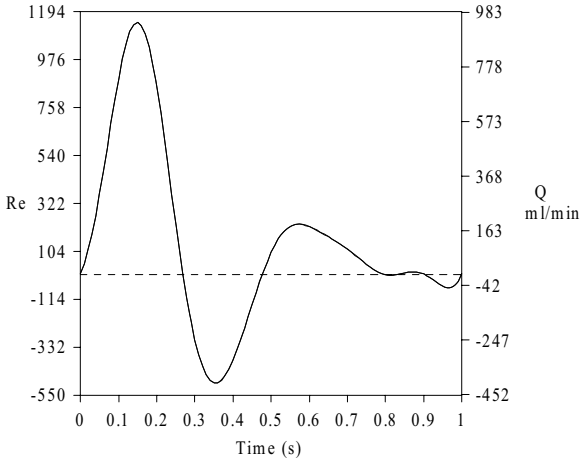

Figure 5: Physiological waveform used for the 3-D anastomosis simulations

5.2 3-D anastomosis

The mid-femoral flow waveform shape as measured by Doppler ultrasonography [Steinman, Vinh, Ethier, Ojha, Cobbold and Johnston (1993)] which is shown in Fig. 5 was specified at the

graft inlet. The physiological flow waveform has a peak systolic flow Reynolds number of 1143 (peak prograde) which is approximately eight times the mean Reynolds number followed by zero flow and a reverse flow of Reynolds number 495 (peak retrograde), approximately three times the mean Reynolds number. Subsequently, the waveform leads to a post diastolic peak followed by zero flow at the end of the cardiac cycle.

No-slip conditions were imposed on all the walls and a zero gauge pressure and zero axial velocity gradients are specified at the distal outlet of the artery.

Blood with a density of 1050 kg/m^3 is used while the viscosity is specified from the non-Newtonian model of Carreau-Yasuda through a user defined function.

6 Results

6.1 2-D end-to-side anastomosis simulations

Velocity profiles under steady flow conditions obtained from numerical analysis are compared with existing experimental data. The axial component of velocity in the 2-D anastomosis model is compared to the experimental measurements at three different axial locations of 0.3, 2.3 and 3.9 respectively in Fig. 6. The axial locations are non-dimensionalized with respect to the channel height. An excellent agreement between the numerical and experimental results is observed at all locations.

Figures 7(a)-(c) show the axial component of velocity under unsteady flow conditions at the same locations identified previously. The comparison with the experiments is carried out at nine different time levels as shown in the figures. A good agreement between the numerical and experimental data is observed at all locations and at different time levels with relatively small discrepancies. Discrepancies are found primarily along the lower wall of the host artery and it was more prominent at the 0.3 location. Quantitative error analysis shows that the relative error ($|(u_{\text{exp}} - u_{\text{num}})|/u_{\text{exp}}$) between the results is around 1-7 % for the entire flow cycle.

Figures 8(a)-(c) show comparison between the

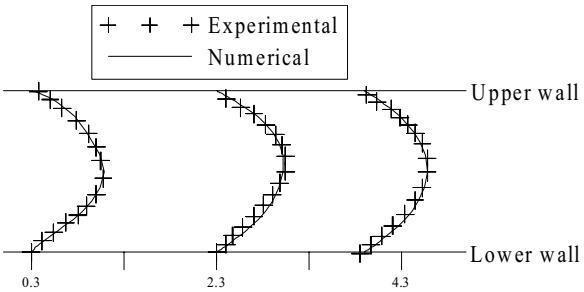

Figure 6: Comparison of the axial velocity component at three representative axial locations (2D, steady case) (a) 0.3; (b) 2.3; (c) 3.9

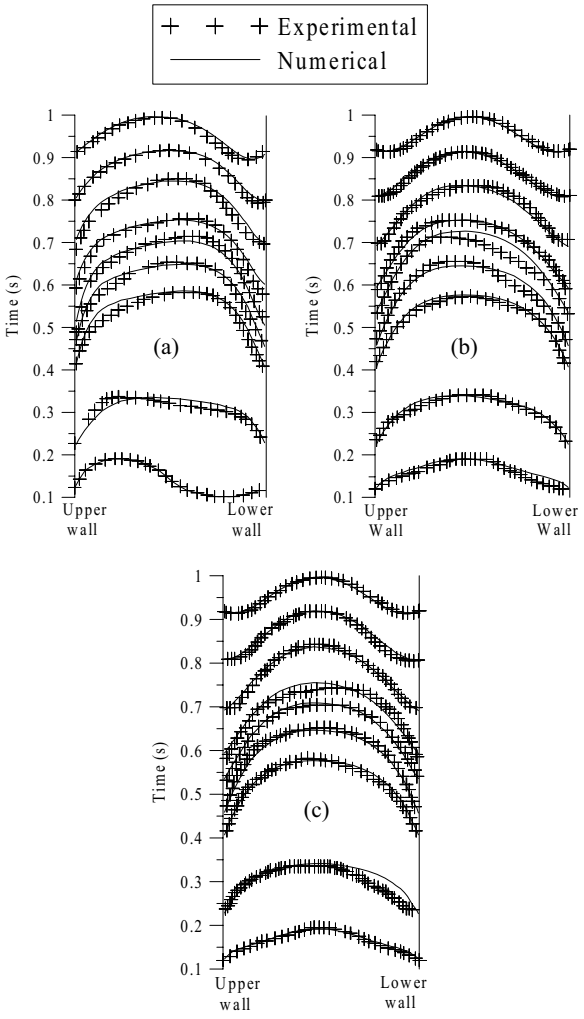

Figure 7: Comparison of the axial velocity component at three representative axial locations (2D, unsteady case) (a) 0.3; (b) 2.3; (c) 3.9

experimental and numerical non-dimensionalized WSS variations at the three non-dimensionalized locations of the host artery through out the flow cycle. WSS's are made dimensionless with respect to ρU^2.

Good to fair agreement between the results are observed with more discrepancies at the lower wall of the host artery. Qualitatively, a general agreement between the numerical and experimental results can be observed throughout the flow cycle for both lower and upper walls. Large discrepancies appear at the lower wall of the anastomosis when compared to the upper wall. The upper wall has the relative WSS errors ($|(\tau_{\text{exp}} - \tau_{\text{num}})|/\tau_{\text{exp}}$) in the range of 1-12 % whereas for the lower wall it ranges from 1% - 35% throughout the flow cycle. The largest relative error appears at the location 0.3 (Fig. 8(a)) for both the lower and upper walls, whereas the locations 2.3 and 3.9 have the second and third highest relative error respectively. This is because at the location 0.3 the flow is more disturbed when compared to other locations. However, this error can partly be reduced by increasing the mesh density at the artery-graft intersection. Furthermore, the large relative errors at the lower wall are the consequence of the corresponding velocity errors (Fig. 7(a)) described previously. Nevertheless, the overall comparison of the shapes of numerical WSS curves follows the experimental curves well. These results and error levels are comparable to those found in the literature [Steinman, Vinh, Ethier, Ojha, Cobbold and Johnston (1993)]. Also, the accuracy of the experimental results was not provided in [Steinman, Vinh, Ethier, Ojha, Cobbold and Johnston (1993)].

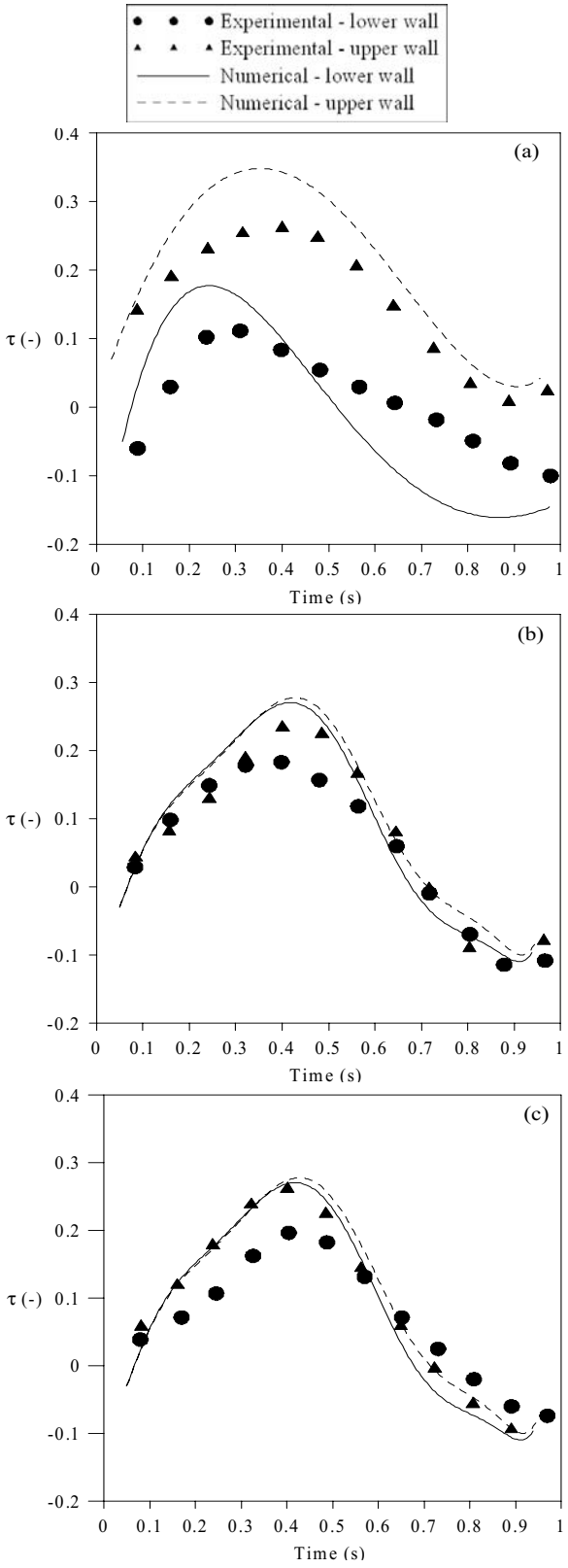

Figure 8: Wall shear stress distributions at three representative axial locations (a) 0.3; (b) 2.3; (c) 3.9

6.2 3-D anastomosis

6.2.1 Flow field

The velocity vectors and streamline patterns on the mid plane for three different time levels which correspond to peak prograde (forward), zero and peak retrograde (backward) flows are shown in Figures 9 (a)-(c) and 10 (a)-(c) respectively.

At peak prograde flow (Fig. 9(a)), the fluid accelerates through the graft and enters the recipi-

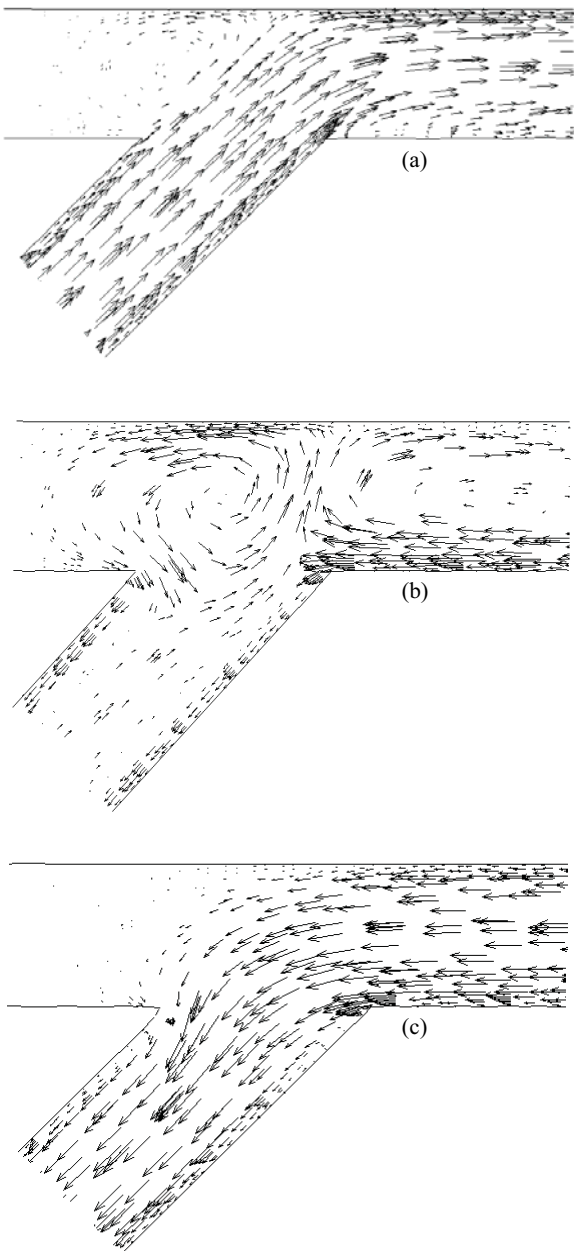

Figure 9: Velocity vectors at the mid section of the 3-D anastomosis for (a) Peak prograde flow (b) Zero (c) Peak retrograde flow

ent artery. There is a significant skewing of the velocity toward the floor of the artery-graft junction due to the entrance of the flow from the graft. The skewing effect of the velocity vectors disappears once the flow progresses downstream of the artery, where the flow becomes fully developed. Separation and a very small recirculating region

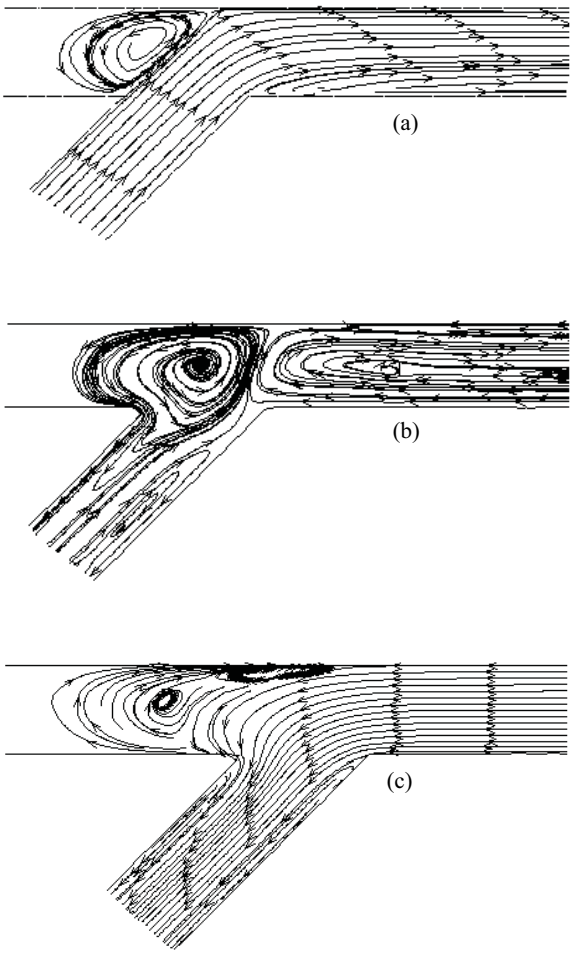

Figure 10: Streamline patterns at the mid section of the 3-D anastomosis for (a) Peak prograde flow (b) Zero (c) Peak retrograde flow

are observed at the toe section of the anastomosis. A large slowly paced vortex in the host artery is evident just proximal to the graft inlet.

At zero flow (Fig. 9(b)), the large vortex observed in Fig. 9(a) just proximal to the graft has continued to grow in size and speed. Furthermore, the vortex at the toe section has grown in size, reaching more than half of the artery diameter. The flow vectors near the walls show that the flow is towards the graft, whereas in the body of the graft the flow is towards the artery.

At peak retrograde flow (Fig. 9(c)), the fluid flow accelerates through the artery, enters the graft and leaves through the artery. The vortex at the downstream location of the anastomosis in zero flow

has disappeared, resulting in a simple flow pattern. However, the vortex at the proximal end which is observed in both prograde and zero flow cases still exists in this flow. Furthermore, a second vortex (Fig. 10 (c)), which was not observed in peak prograde and zero flow, is evident at the hood section of the artery.

6.2.2 Wall shear stress

Wall shear stress distribution at the distal anastomosis is of importance with regard to intimal thickening. Figures 11 and 12 represent the variation of the WSS over the upper wall (hood section) and lower wall (toe and heel section) of the artery for three different time levels which correspond to peak prograde (forward), zero and peak retrograde (backward) flows. The differences in the velocity field at the anastomosis due to three different flows give rise to distinct WSS patterns.

In Fig. 11, the region of large increased axial WSS observed in the peak prograde flow of the cycle at graft-artery junction is due to the impingement of the bypass flow from the graft to the hood of the artery. From that point, the shear stress drops sharply over a narrow section of the artery where the flow splits and proceeds smoothly along the artery. The negative shear stress at the upstream location of the anastomosis indicates the flow reversal and is related to the recirculation in that region. The reduction of flow disturbances downstream of the artery suggests the smooth flow behavior which is confirmed by the constant value of WSS. Figure 12 illustrates the elevated shear stresses at the toe and heel portion of the anastomosis. The negative shear stress at the toe portion suggests a recirculation region. WSS patterns for the zero and prograde flows follow the same pattern as peak prograde flow with less intensity in magnitude. WSS's are identical at the heel location for prograde and retrograde flows.

6.2.3 Wall shear stress gradient

The magnitude of WSSG in a uniform flow region is by definition zero. If the WSSG value is other than zero, it denotes a non-uniform flow behavior. In order to illustrate a quantitative comparison between the three flows, the magnitudes of WSSG along the hood of the artery is shown in Fig.13. Figure 13 shows the WSSG values only in the anastomosis region, since beyond that region the values are zero denoting a uniform flow. There exists a local high axial WSSG as well as a local low axial WSSG on the artery wall for all cases. The magnitude of WSSG in the anastomosis region is greatly increased in the prograde flow. This indicates existence of a large variation in the shear stresses along the artery, which is further confirmed from Fig. 11, in which the variation appears from high negative value to a high positive value. However, WSSG magnitude in the other two cases remains almost identical following the general trend of prograde flow with lower magnitude.

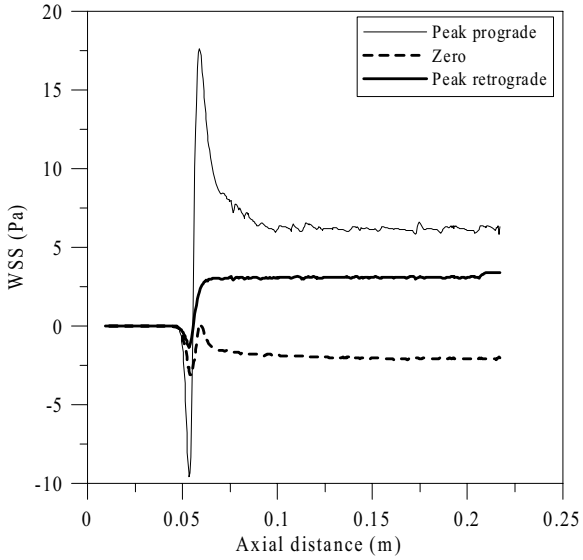

Figure 11: Wall shear stress along the artery hood for the three time levels

7 Discussions and conclusions

Intimal hyperplasia is a common cause of failure in arterial bypass surgery leading to restenosis and graft failure. Numerous researchers have reported qualitative analogy between IH and the hemodynamic variables. Variables such as low WSS, high WSS, oscillatory WSS, and spatial and temporal WSSG are used to correlate the regions

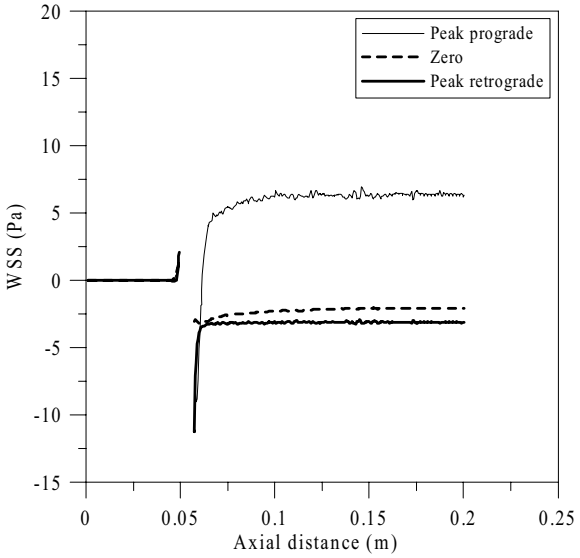

Figure 12: Wall shear stress along the lower wall of the artery for the three time levels

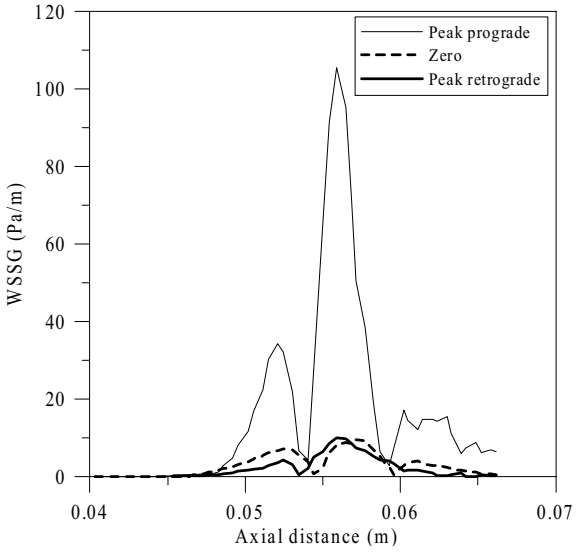

Figure 13: Wall shear stress gradient along the artery hood for the three time levels

susceptible for IH. In order to understand the relationship between these variables and the development of IH, numerous investigations have been conducted both experimentally and numerically, to predict the relation between IH and specific hemodynamic variables. Quantitative assessment of the numerical tools with the vitro or vivo experiments is necessary. In the current investigation, comparison of numerical results with available experimental data under pulsatile flow conditions were conducted to validate the numerical tool used. While using the numerical tool, various options of solving the governing equations were attempted and the solutions which provided minimal errors are shown. The same procedure is extended to 3-D to predict the development of IH in 3-D anastomosis. The non-Newtonian model which is utilized in this study has been validated for accuracy [Shaik, Hoffmann and Dietiker (2007)].

Comparison of numerical results with the experimental data for steady and pulsatile flows shows excellent agreement in steady flow, and minor discrepancies in pulsatile flows. The main cause for the discrepancies can be attributed to the way the spline is fitted to the limited amount of experimental data points. Moreover, while performing these experiments authors neglected 3-D effects which could explain the error levels in the velocity profiles. Discrepancies found in WSS comparison follow the same explanation. The high percentage of error may be attributed to the sensitivity of shear stress towards the variation in the velocity profiles.

We extended the work from 2-D to 3-D model and implemented the Carreau-Yasuda model to account for non-Newtonian property of blood to study the effect of hemodynamics in the anastomosis of a vascular bypass graft. While extending the work, importance has been given to reduce the discrepancies in WSS which were seen in 2-D model of anastomosis. This reduction is performed by employing a finer aspect ratio mesh than the 2-D model. Moreover, meshes are clustered near the anastomosis arterial wall to produce a greater accuracy in calculating the shear stress. Furthermore, the mid-femoral waveform, which was used as the inlet condition has been fitted to the measured waveform with many data points to reduce the error levels in both velocity and WSS profiles found in 2-D model.

The pulsatile simulations of 3-D anastomosis clearly show the elevated and the negative WSSs at the toe, heel and hood regions of the artery-graft anastomosis. Similar conclusion can be attributed by considering the distribution of WSSG along

the artery wall. The same behavior is observed for the other two flow times in the cycle with a slight decrease in the magnitude of the stresses. The region where the WSS is negative corresponds to the recirculation region within the artery. Regions of reverse flow or recirculating flows are usually associated with local deposit of particles, which results in a blockage of the artery, leading to IH [Weston, Rhee and Tarbell (1996)]. The findings are consistent with the works of Steinman, Vinh, Ethier, Ojha, Cobbold and Johnston (1993), Ojha (1993), Ojha, Ethier, Johnston and Cobbold (1990), and Bassiouny, White, Glagov, Choi, Giddens and Zarins (1992). The elevated and negative WSS which leads to the development of IH at the artery-graft junction has to be reduced or eliminated by considering design variations in the anastomosis geometry. In summary, the hemodynamics within the artery-graft anastomosis may significantly affect the development of IH. Potential artery-graft anastomosis design improvements that reduce the amount of WSS may have to be performed in order to increase the clinical success of vascular bypass grafts.

References

1. **Ku, D. N.; Allen, R. C.** (1995): *Vascular grafts in the biomedical engineering handbook*, Boca Raton, FL, CRC Press, Inc., pp. 1871-1878.

2. **Dilley, R. J.; McGeachie, J. K.; Prendergast, F. J.** (1998): A review of the histologic changes in vein-to-artery grafts with particular reference to intimal hyperplasia. *Arch. Surg.*, vol. 123, pp. 691-696.

3. **Echave, V.; Koornick, A. R.; Haimov, M.** (1979): Intimal hyperplasia as a complication of the use of the polytetrafluoroethylene graft for femoral-popliteal bypass. *Surgery*, vol. 86, pp. 791-798.

4. **Sottiurai, V. S.; Yao, J. S.; Baston, R. C.; Sue, S. L.; Jones, R.; Nakamura, Y. A.** (1989): Distal anastomotic intimal hyperplasia: Histopathologic character and biogenesis. *Annu. Vasc. Surg.*, vol. 15, pp. 708-717.

5. **Clowes, A. W.; Kirkman, T. R.; Clowes, M. M.** (1986): Mechanism of arterial graft failure. II. Chronic endothelial and smooth muscle cell proliferation in healing PTFE prostheses. *J. Vasc. Surg.*, vol. 3, pp. 877-884.

6. **Bandyk, D. F.; Seabrook, G. R; Moldenhauer, P.** (1988): Hemodynamics of vein graft stenosis. *J. Vasc. Surg.*, vol. 8, pp. 688-695.

7. **Clowes, A. W.; Clowes, M. M.** (1980): The influence of hypertension on injury-induced myointimal thickening. *Surgery*, vol. 88, pp. 254-259.

8. **Dobrin, P. B., Littooy, F. N., and Endean, E. D.** (1989): Mechanical factors predisposing to intimal hyperplasia and medial thickening in autogenous vein grafts. *Surgery*, vol. 105, pp. 393-400.

9. **Rittgers, S. E.; Karayannacos, P. E.** (1978): Velocity distribution and intimal proliferation in autologous vein grafts in dogs. *Circ. Res.*, vol. 42, pp. 792-801.

10. **Chevru, A.; Moore, W. S.** (1990): An overview of intimal hyperplasia. *SG & O.*, vol. 171, pp. 433-447.

11. **Rittgers, S. E.; Bhambhani, G. H.** (1991): Pulsatile flow in a modeled bypass graft anastomosis using doppler color flow mapping. Biomechanics Symposium., *ASME AMD.*, vol. 120, pp. 21-24.

12. **Keynton, R. S.; Evancho, M. M.; Sims, R. L.; Rittgers, S. E.** (1999): The effect of graft caliber upon wall shear within in vivo distal vascular anastomosis. *J. Biomech. Eng.*, vol. 121, pp. 79-88.

13. **Keynton, R. S.; Rittgers, S. E.; Shu, M. C. S.** (1991): The effect of angle and flow rate upon hemodynamics in distal vascular graft anastomosis: An in vitro model study. *J. Biomech. Eng.*, vol. 113, pp. 458-463.

14. **Loth, F.; Jones, S. A.; Giddens, D. P.; Bassiouny, H. S.; Zarins, C. K.; Glagov, S.** (1997): Measurement of velocity and wall shear stress in a PTFE vascular graft model under steady flow conditions. *J. Biomech. Eng.*, vol. 119, pp. 187-194.

15. **Steinman, D.; Vinh, B.; Ethier, C.; Ojha, M.; Cobbold, R.; Johnston, K.** (1993): A numerical study of flow in a two-dimensional end-to-side anastomosis model. *J. Biomech. Eng.*, vol. 115, pp. 112-118.

16. **Pietrabissa, R.; Inzoli, F.; Fumero, R.** (1990) Simulation study of the fluid dynamics of aorta-coronary bypass. *J. Biomed. Eng.*, vol. 12, pp. 419-428.

17. **Perktold, K.; Tatzl, H.; Schima, H.** (1993): Computer simulation of hemodynamic effects in distal vascular graft anastomosis. Advances in Bioengineering, *ASME BED.*, vol. 26, pp. 91-94.

18. **Ojha, M.** (1993): Spatial and temporal variations of wall shear stress within an end-to-side arterial anastomosis model. *J. Biomech.*, vol. 26, pp. 1377-1388.

19. **Ojha, M.; Ethier, C.; Johnston, K.; Cobbold, R.** (1990): Steady and pulsatile flow fields in an end-to-side arterial anastomosis model. *J. Vasc. Surg.*, vol. 12, pp. 747-753.

20. **Bassiouny, H. S.; White, S.; Glagov, S.; Choi, E.; Giddens, D. P.; Zarins, C. K.** (1992): Anastomotic intimal hyperplasia: mechanical injury or flow induced. *J. Vasc. Surg.*, vol. 15, pp. 708-716.

21. **Bharadvaj, B. K.; Daddario, D. M.** (1982): Flow studies at arterial anastomosis. Proc. 35th ACEMB, Philadelphia.

22. **Fei, D. Y.; Thomas, J. D.; Rittgers, S. E.** (1994): The effect of angle and flow rate upon hemodynamics in distal vascular graft anastomosis. *J. Biomech. Eng.*, vol. 116, pp. 331-336.

23. **Henry, F.; Collins, M.; Hughes, P.; How, T.** (1996): Numerical investigation of steady flow in proximal and distal end-to-side anastomosis," *J. Biomech. Eng.*, vol. 118, pp. 302-310.

24. **Lei, M.; Archie, J. P.; Kleinstreuer, C.** (1997): Computational design of a bypass graft that minimizes wall shear stress gradients in the region of the distal anastomosis. *J. Vasc. Surg.*, vol. 25, pp. 637-646.

25. **Lei, M.; Archie, J. P.; Kleinstreuer, C.** (1996): Geometric design improvements for femoral graft-artery junctions mitigating restenosis. *J. Biomech.*, vol. 29, pp. 1605-1614.

26. **Kleinstreuer, C.; Lei, M.; Archie, J. P.** (1996): Flow Input Waveform Effects on the Temporal and Spatial Wall Shear Stress Gradients in a New Femoral Graft-Artery Connector. *J. Biomech. Eng.*, vol. 118, pp. 506-510.

27. **Yang, C.; Tang, D.; Liu, S. Q.** (2003): A Multi-Physics Model with Fluid-Structure Interactions for Blood Flow and Restenosis in Rat Vein Grafts. *Computers and Structures*, vol. 81, pp. 1044-1058.

28. **Chien, S.; Usami, S.; Richard, S.** (1984): Blood flow in small tubes. Hand book of physiology, Section 2: the cardiovascular system, microcirculation part I. *Amer. Physio. Soc.*, Bethesda MD, vol. IV, pp. 217-249.

29. **Quemada, D.** (1977): Rheology of concentrated disperse systems: general features of the proposed non-Newtonian model comparison with experimental data. *J. Rheolo. Acta.*, vol. 17, pp. 643-652.

30. **Yeleswarapu, K. K.** (1996): Evaluation of continuum models for characterizing the constitutive behavior of blood in: *Ph.D. thesis*, Department of Mechanical Engineering, University of Pittsburgh.

31. **Shaik, E.; Hoffmann, K. A.; Dietiker, J-F.** (2006): Numerical flow simulations of blood in arteries. AIAA-2006-0294.

32. **Gijsen, F. G. H.; Van de Vosse, F. N.; Janssen, J. D.** (1999): The Influence of the non-Newtonian properties of blood on the flow in large arteries: steady flow in a carotid bifurcation model. *J. Biomech.*, vol. 32, pp. 601-608.

33. **Shaik, E.; Hoffmann, K. A.; Dietiker, J-F.** Numerical experiments on the effects of artery-graft compliance mismatch using fluid-structure interactions. *J. App. Biomechanics*, Submitted for publication.

34. **Weston, M. W.; Rhee, K.; Tarbell, J. M.** (1996): Compliance and diameter mismatch affect the wall shear rate distribution near an end-to-end anastomosis. *J. Biomech.*, vol. 29, pp. 187-198.